Biosensors and Bioelectronics 312 (2026) 119049

Contents lists available at ScienceDirect

Biosensors and Bioelectronics

journal homepage: www.elsevier.com/locate/bios

A one-tube autocatalytic transcription-driven CRISPR cascade for ultrasensitive mRNA detection

Yuqian Tan [a,1], Xin He [a,1], Erzhu Shao [a], Qiang Chen [a], Li Zhang [b,*], Shixiong Deng [a,**]

[a] Department of Forensic Medicine, Chongqing Medical University, Chongqing, 400016, China
[b] Key Laboratory of Laboratory Medical Diagnostics, Ministry of Education, Department of Laboratory Medicine, Chongqing Medical University, Chongqing, 400016, China

ARTICLE INFO

Keywords:
Autocatalytic CRISPR
Three-way junction
Positive feedback circuits
OR-gate
Multiplex

ABSTRACT

The rapid identification and precise quantification of cancer biomarkers are essential for the purposes of diagnosis, classification, and therapeutic intervention. Traditional molecular diagnostic methodologies, such as polymerase chain reaction (PCR), provide considerable sensitivity; however, they depend on exponential amplification and advanced instrumentation, thereby constraining their applicability for point-of-care testing. In this study, we developed a Transcription-driven CRISPR Cascade Amplification (TCCA) for one-tube detection of mRNA at the concentration of 0.6 copies/μL within just 30 min. The target-induced assembly of a three-way junction (TWJ) facilitates the generation of a split T7 promoter, which initiates transcription and activates Cas13a collateral cleavage. The activated Cas13a subsequently cleaves cascade probes and releases new trigger strands, forming a transcription-driven cascade amplification circuit. The assay enables multiplex detection of breast cancer–associated mRNA biomarkers (HBB, KRT17, and CD55) in cell lysates, demonstrating robust performance in intricate biological matrices. Furthermore, incorporation of a multiplex OR-gated logic design enables parallel target recognition, thereby enhancing detection reliability for rapid and accurate clinical diagnostics.

1. Introduction

Messenger RNA (mRNA) serves as a direct indicator of gene expression dynamics and cellular functional states. In breast cancer, aberrant mRNA expression profiles are closely associated with tumor subtypes, progression, and therapeutic response, highlighting their potential as informative biomarkers for molecular classification and early diagnosis (Hohmann et al., 2025). Conventional nucleic acid diagnostics typically rely on polymerase chain reaction (PCR) or other enzymatic amplification methods to achieve high analytical sensitivity. Despite their high efficacy, workflows based on exponential amplification are often constrained by prolonged reaction times and strong dependence on sophisticated instrumentation, which limit their applicability in point-of-care settings (Aslan et al., 2026; Kreitmann et al., 2023).

CRISPR-based biosensing systems have solved several technical bottlenecks by providing programmable target recognition and robust operation under isothermal conditions (Wang et al., 2025). By leveraging their collateral activities to cleave reporter containing fluorophores and quenchers, detectable signals can be generated. Among these, Cas13a, a type VI CRISPR-associated protein, is capable of recognizing target-specific RNA sequences and degrading adjacent single-stranded RNA, rendering it exceptionally versatile for diagnostic applications (Tong et al., 2024). Nevertheless, most current CRISPR-based assays depend on pre-amplification step to achieve clinical sensitivity (He et al., 2025; Zhao et al., 2025). As an innovative strategy, autocatalytic CRISPR architectures directly combines initial target identification with the feedback-driven signal propagation, thereby minimizing the necessity for pre-amplification (Shi et al., 2021). Numerous cascade probe strategies have been devised to facilitate conditional activation, corroborating that nucleic-acid structures can be programmed as feedback gates to drive autocatalytic reactions (Lim, n. d.). However, the dependence on multiple effective Ribonucleoprotein (RNP) complexes and insufficient control over Cas enzyme activation underscore the need for an upstream regulatory mechanism that can

* Corresponding author.
** Corresponding author.
E-mail addresses: lizhang@cqmu.edu.cn (L. Zhang), dengshixiong@cqmu.edu.cn (S. Deng).
[1] These author contributed equally to this work.

https://doi.org/10.1016/j.bios.2026.119049
Received 30 April 2026; Received in revised form 9 July 2026; Accepted 18 July 2026
Available online 19 July 2026
0956-5663/© 2026 Elsevier B.V. All rights are reserved, including those for text and data mining, AI training, and similar technologies.

impose kinetic constraints and suppress background activation (Zhang et al., 2023). Compared to 3′-hydroxyl–driven DNA polymerases, T7 RNA polymerase exhibits higher specificity through strict promoter dependence (Gholamalipour et al., 2018; Schaffter et al., 2018). In this regard, transcription-based mechanism offers a promising strategy for improving reaction fidelity and system integration.

Herein, we integrate a split-T7 promoter with CRISPR-Cas13a cascade probe system, to establish a novel analytical strategy. Effective RNP assembly and feedback initiation are governed by coordinated multi-component release, functionally imposing an AND-gated activation requirement. In parallel, an OR-gated input recognition module ensures the presence of any target biomarker (HBB, CD55, and KRT17) can generate a detectable signal. This hierarchical logic-guided architecture combines stringent activation control with broadened detection coverage, resulting in improved assay robustness and enhanced signal-to-noise performance. The detection reaction can be completed within 30 min at 37 °C while effectively suppressing background signals. Finally, the practically applicability of the proposed platform is validated by assessing its detection performance in breast cell line.

2. Experimental section

2.1. Materials and chemicals

LwaCas13a together with the 10× Cas13a reaction buffer was sourced from Magigen. T7 RNA polymerase, 10× transcription buffer, rNTPs, RNase inhibitor, DNase I, and diethylpyrocarbonate (DEPC)-treated water were provided by Sangon Biotech (Shanghai, China). The 5× DNA loading buffer was supplied by Biosharp (Anhui, China). The 20 bp DNA ladder and GelRed nucleic acid stain were obtained from Takara Bio (Dalian, China). RNA isolater Total RNA Extraction Reagent, Beyo-Fast™ SYBR Green qPCR Mix (2×), and the First-Strand cDNA Synthesis Kit were from Beyotime (Shanghai, China), whereas the RNA Clean Kit was obtained from Tiangen Biotech (Beijing, China). The oligonucleotide sequences employed in this study are summarized in Table S1.

2.2. Real-time fluorescence monitoring and gel electrophoresis analysis

The cascade probe was prepared prior to the detection assay. Briefly, the cascade probe was diluted in 1× Cas13a reaction buffer and pre-incubated at room temperature for 6 h to ensure the formation of a stable dumbbell configuration. The preincubated cascade probe was then used as a stock reagent in subsequent detection reactions and stored at −20 °C. To assemble the TWJ complex, 100 nM each of the SP1, SP2, and ST oligonucleotides were mixed with varying target concentrations in a 10× Cas13a reaction buffer. The mixture was subjected to thermal denaturation at 95 °C for 5 min, followed by gradual cooling to room temperature, and stored at 4 °C for use.

For the standard reaction, the reaction was carried out in a 20 μL mixture consisting of two components: the CRISPR mixture and the TWJ mixture, both of which were prepared on ice.

The ribonucleoprotein (RNP) complex, comprising 20 nM LwaCas13a and 20 nM crRNA in 1× Cas13a buffer, was pre-incubated at 0 °C for 10 min. Then, the final reaction matrix consisted of 20 nM Cas13a, 20 nM crRNA, 5 nM each of SP1, SP2, and ST, 5 nM cascade probe, 1 mM NTPs, 1× transcription buffer, 1× Cas13a reaction buffer, 250 nM RNA reporter, 20 U T7 RNA polymerase, 20 U RNase inhibitor, and DEPC-treated H_2O added to 20 μL. Reactions were carried out on a CFX 96 Real-Time PCR Detection System (Bio-Rad, USA) at 37 °C, with fluorescence recorded every 30 s. Each condition was tested in at least three independent replicates to evaluate reproducibility. The reliability of fluorescence readouts was further verified by 12% polyacrylamide gel electrophoresis (PAGE). For gel analysis, 5 μL of reaction product was mixed with 1 μL of 6× loading buffer prior to electrophoretic separation. Electrophoresis was conducted at a constant 110 V for 60 min. The gel was then stained with Gel Red at room temperature for 20 min and visualized under UV illumination using the ChemiDoc XRS imaging system (Bio-Rad, USA).

2.3. RNA synthesis

Forward and reverse DNA templates for in vitro transcription (IVT) were rationally designed according to the corresponding RNA sequences (Table S1). To prepare the double-stranded transcription templates, the forward (unRNAsense) and reverse (unRNAantisense) oligonucleotides (25 μM each) were mixed at an equimolar ratio (1:1) in 1× transcription buffer. The mixture was thermally denatured at 90 °C for 5 min and subsequently subjected to a controlled cooling ramp of 0.5 °C/s down to 25 °C to facilitate complete hybridization. The annealed duplexes were then utilized for the IVT reaction, which was carried out at 37 °C for 8 h. Following transcription, 5 μL of DNase I was introduced into the 20 μL reaction matrix and incubated at 37 °C for 1 h to completely degrade the residual DNA templates. The generated RNA products were purified using a Total RNA Clean Kit (Tiangen Biotech, Beijing, China). Finally, the RNA concentration was quantified with NanoDrop 2000c spectrophotometer, and the purified aliquots were stored at −80 °C prior to subsequent assays.

2.4. Application of cell lines

The human non-invasive breast cancer cell line (MCF-7) and the human invasive breast cancer cell line (MDA-MB-231) used in this study were cultured in high-glucose Dulbecco's Modified Eagle Medium (DMEM). The culture medium was prepared by adding 10% (v/v) fetal bovine serum (FBS) and 1% (v/v) penicillin–streptomycin to the basal medium. Cells were routinely cultured at 37 °C in a humidified incubator with a controlled 5% CO_2 atmosphere, and maintained under standard sterile conditions throughout the experiments.

2.5. RT-PCR assay

Quantitative reverse transcription PCR (qRT-PCR) was employed as a reference method for circulating mRNA analysis. Thermal cycling conditions consisted of an initial denaturation at 95 °C for 2 min, followed by 40 cycles of denaturation at 95 °C for 5 s and annealing/extension at 60 °C for 30 s. Each 20 μL reaction contained 10 μL 2× SYBR Green qPCR Mix, 2 μL forward primer (3 μM), 2 μL reverse primer (3 μM), 2 μL cDNA, and 6 μL DEPC-treated water. Reverse transcription of extracted mRNA was performed using First-strand cDNA Synthesis. Amplification was carried out on a real-time quantitative PCR instrument with SYBR Green chemistry, using β-actin as the internal reference gene. Cycle threshold (CT) values were converted to HBB/CD55/KRT17 concentrations based on standard curves generated from synthetic HBB/CD55/KRT17 templates.

2.6. Statistical analysis

Statistical analyses were conducted by GraphPad Prism (GraphPad Prism Inc., California, USA) and SPSS Statistics (IBM Corporation, New York, USA). Significance levels were denoted as follows: $P < 0.001$ (***), $P < 0.01$ (**), and $P < 0.05$ (*).

3. Results and discussion

3.1. Conceptual framework of the method

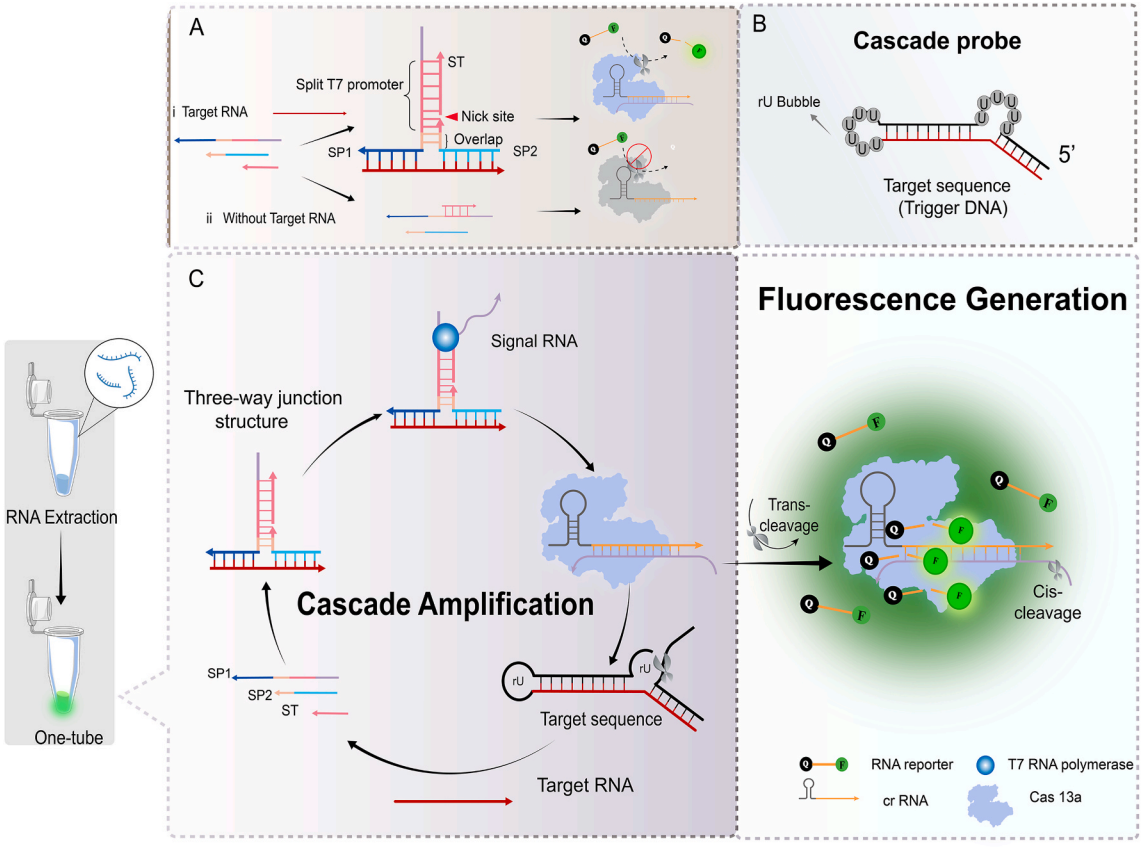
Reported study has revealed that the analytical sensitivity of LwaCas13a assays is primarily constrained by its inherently low trans-cleavage turnover rate (kcat ≈ 1) and the restricted formation of activated RNP complexes, which is determined by the availability of target molecules (Fakhr et al., 2026; Son et al., 2026). At low analyte concentrations, the generated fluorescent signal becomes indistinguishable

from instrumental and background noise, fundamentally limiting the signal-to-noise (S/N) ratio before the enzymatic substrate is depleted (Huyke et al., 2022). Although the incorporation of exponential amplification enhanced the detection sensitivity, it not only generally accompanied by high background signals but also rend the CRISPR reaction redundant (Zhang et al., 2025; Zhou et al., 2024, 2026).

Here, we proposed a proximity-induced Transcription-driven CRISPR Cascade Amplification (TCCA) to circumvent sensitivity limitations (Scheme 1). The TCCA reaction system is consist of three interrelated modules: (i) target-induced assembly of three-way junction (TWJ) DNA probes, (ii) transcriptional amplification based on split T7 promoter, and (iii) CRISPR/Cas-mediated signal amplification coupled with cascade probe-driven positive feedback.

The transcriptional amplification reaction utilizes three DNA reaction probes as target recognition elements including SP1, SP2 and ST. Among them, SP1 is organized into three functional segments, including a transcriptional template (purple region), a T7 promoter fragment (pink region), an overlap sequence (yellow region) and a partial target recognition sequence (dark blue region). Meanwhile, ST possesses a partial sequence of the T7 promoter (pink region), which hybridizes with SP1 to form the double-stranded T7 promoter containing a nick site. Besides, the sequences on SP2 are composed of a partial T7 promoter segment (pink region), an overlap region complementary to SP1 (yellow region) together with a target recognition sequence (light blue region). To enable stable promoter reconstitution only upon target-triggered assembly, an overlap sequence was introduced between SP1 and the split T7 promoter segment on SP2, allowing the hybridization stability to be precisely regulated through the melting temperature (Tm). In the absence of target, TWJ probes remain unassembled, as region of the overlap exhibits a low Tm of 11 °C, which is insufficient to support stable hybridization at 37 °C. Consequently, the weak interaction between SP1 and SP2 fail to support reconstruction of the complete nicked T7 promoter. Upon target binding, the target-guided assembly of the TWJ spatially confines SP1, SP2, and ST, markedly increasing their effective local concentration and stabilizing the structure. This cooperative assembly enables the formation of a stable split double-stranded T7 promoter that can be efficiently recognized by T7 RNA polymerase (Scheme 1A). Moreover, the designed cascade probe is constructed with two functional domains. Each loop domain contains an rU–rU sequence which can be cleaved by an activated Cas13a, and a trigger DNA strand identical to the target recognition sequence is sequestered in the stem region (Scheme 1B).

As shown in Scheme 1C, the presence of the target drives the self-assembly of the three-way junction, generating a complete transcription template which can generate the signal RNA of downstream CRISPR/Cas13a system by the help of T7 RNA polymerase. Upon recognition of the signal RNA, the RNP complex cleaves signal RNA in cis and activates its trans activity. Then the RNP complex cleaves the single-stranded RNA bulge embedded in the cascade probe and releases trigger DNA strand by the exposure of complementary sequences, leading to the formation of additional TWJ structure. In this way, newly formed TWJ structures generate additional activated RNPs via the same mechanism, leading to further cleavage of ssRNA bulge regions and release of trigger DNA strands, thereby enabling the subsequent amplification round. This autocatalytic process establishes a feedback-driven signal amplification network. Importantly, this amplification mechanism is governed by autocatalytic cascade reaction instead of initial target concentration, enabling even a few targets to generate a robust fluorescent intensity. All processes were conducted in a single tube. Every DNA probe or cascade probe was optimized using NUPACK (Zadeh et al., 2011) to minimize unintended hybridization (Table S1).



Scheme 1. Schematic diagram of the cascade reaction. (A) The progress of TWJ transcription. (B) The structure of cascade probe. (C) Principle of RNA detection based on a Cas13a-driven catalytic positive feedback circuit.

3.2. Feasibility of the platform

To demonstrate the feasibility of the method, we confirmed the target-triggered assembly of the three-way junction (TWJ). Given that the formation of a nicked double-stranded T7 promoter is the critical step in TCCA, the split ratio of the T7 promoter was optimized first (Kim et al., 2024; Li et al., 2025). To this end, the split site was systematically shifted along the promoter sequence from the 5′ end, generating a series of split promoter at various ratios (Scheme 1A). By incorporating the complementary sequence of the crRNA into the template, the transcription process could be monitored via the fluorescence signal derived from activated CRISPR/Cas13a. Five groups of reaction probes were incorporated into T7 promoter transcription templates with different split configurations, designated as 1/19, 2/18, 3/17, 4/16, and 5/15 (Fig. S2A). When the split ratio ranged from 1/19 to 3/17, efficient transcription occurred with target. By contrast, in the case of ST + SP1, the results showed markedly reduced fluorescence, indicating the lack of sequences at the 5′ end of the T7 promoter could impair transcriptional activity. Additionally, the usage of the 3/17 split configuration markedly reduced the fluorescence in the presence of SP1+ST, implying that the three-nucleotide portion on the 5′ side of the T7 promoter was vital for specific recognition by T7 RNA polymerase. Conversely, minimal transcription was observed with the 5/15 split configuration despite the presence of all key components, suggesting that placement of a nick five nucleotides from the 5′ end disrupts promoter recognition. Based on these observations, the 3/17 split configuration was selected for integration with the three-way junction design. Given the critical role of the complementary overlap between SP1 and SP2 in TWJ assembly, the overlap length was further optimized. The S/N peaked at a complementary length of 6 nucleotides, whereas further extension to 7 nucleotides led to nonspecific transcription even without the target. Consequently, the new overlap was defined as 3 bp, resulting in a total complementary overlap of 6 bp (Fig. S2B).

To verify the feasibility of the TCCA system, real-time fluorescence was monitored under various reaction condition. In Fig. 1A, negligible signals were observed in the absence of key components, whereas the group including SP1 and SP2 with target produced strong signal, demonstrating their indispensable roles in the reaction. Besides, melting curve analysis further validated reaction products. As shown in Fig. S3, there were two characteristic peaks detected only in the positive control group containing target, while none of them was observed from the negative control.

The observations were further confirmed by 12% polyacrylamide gel electrophoresis (PAGE) analysis. As shown in Fig. 1B, in the absence of the target, no combination of the reaction strands was observed (lane 4). By contrast, upon addition of the target to all reaction probes, the three-way junction structure occurred, showing a new gel band with the lowest electrophoretic mobility (lane 5). In the presence of T7 RNA polymerase, substantial signal RNA generated (lane 6), accompanied by the disappearance of bands corresponding to SP1 and SP2, which successfully indicated that the target could trigger the three-way junction self-assembly and initiates transcription. Subsequently, we employed another PAGE analysis to confirm the construction of the TCCA. As shown in Fig. S4, the cascade probe band disappeared in the presence of the target, with appearance of new bands exhibiting increased electrophoretic mobility.

In addition, we confirmed that the targeted-activated RNP could cleave single-stranded RNA bulges and release functional products. Nondenaturing PAGE confirmed the time-dependent trans cleavage of cascade probe by activated RNP (Fig. 1C). Lane 1–2 included 1) the 20 bp DNA ladder, 2) cascade probe (1 μM), Lane 3–6 represented trans-cleavage reactions at 0, 5, 30, and 60 min. At 30 min (lane 5), partial

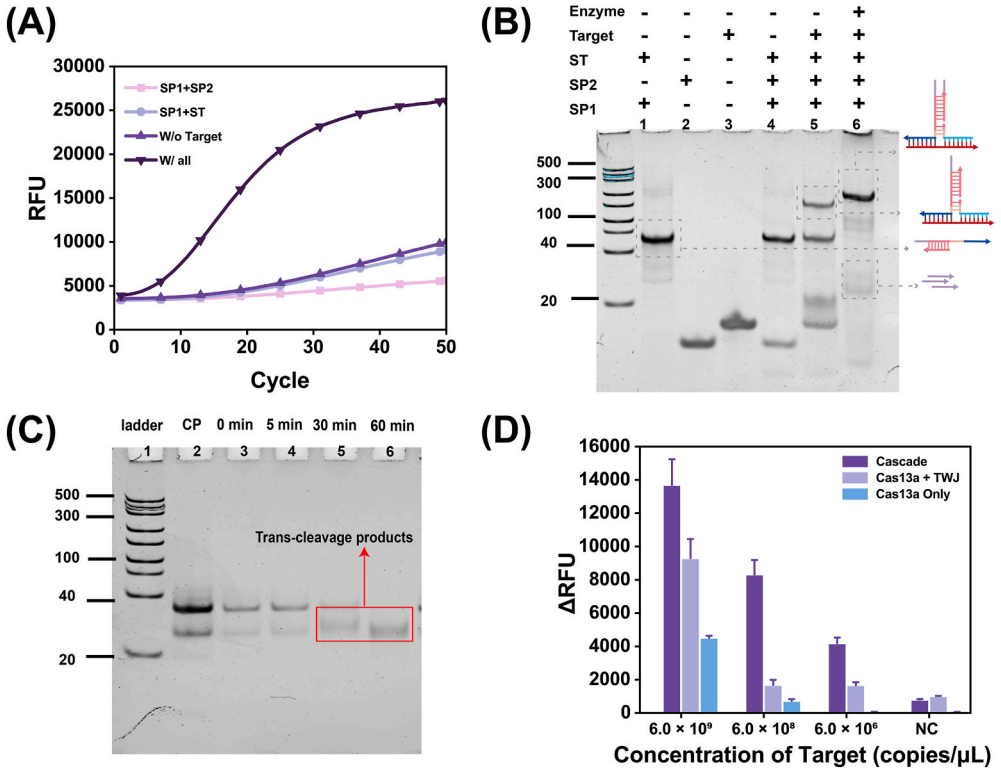


Fig. 1. Feasibility of TCCA. (A) Fluorescence intensity under different reaction conditions. The inset provides an expanded view of signals obtained from reactions containing partial combinations of components. (B) Gel electrophoresis characterization of transcription reaction components and products. The transcription reactions were carried out at 37 °C for 30 min, and SP1, SP2, ST, and target were at 100 nM. (C) The trans-cleavage activity of the activated RNP toward cascade probe was examined by nondenaturing PAGE analysis, and the electrophoresis was performed at 110 V for 60 min. (D) Comparison of different reaction systems. The reaction components were incubated with the HBB target fragment at 37 °C for 30 min to obtain fluorescence signal. Error bars: standard deviation (SD), n = 3.

cascade probe cleavage conducted smaller DNA fragments. As incubation proceeded (lane 6), the cascade probe bands gradually diminished in intensity, accompanied by the accumulation of lower molecular weight fragments. As shown in Fig. S5, the downstream fluorescence signal progressively increased with extended pre-cleavage time, confirming that released trigger strands generated by activated RNP efficiently initiate the downstream cascade reaction. Collectively, these results demonstrate that TWJ assembly triggers transcription, while activated Cas13a drives cascade probe cleavage and amplify the signal.

To further evaluate the advantages of the system in improving detection performance, signals from the cascade reaction, single Cas13a system, and TWJ-assisted Cas13a system were compared at target concentrations of 6×10^9 copies/μL, 6×10^8 copies/μL, and 6×10^6 copies/μL. Robust signals were observed at 6×10^9 copies/μL and 6×10^8 copies/μL for all systems. As shown in Fig. 1D, the single Cas13a system produced signals indistinguishable from the negative control in 6×10^6 copies/μL, reflecting the intrinsic limitation of Cas13a due to the restricted number of activated RNP complexes at low target abundance. Incorporation of the transcription module modestly improved sensitivity, but the TWJ-assisted system still exhibited limited discrimination. In contrast, the cascade system maintained clear signal separation from the negative control, demonstrating its superior detection performance at low target concentrations.

3.3. Cascade reaction optimization

To establish the optimal reaction conditions and maximize discrimination between positive and negative groups, we systematically optimized the key reaction parameters. The positive groups are represented by dark columns, while negative groups are demonstrated in light. As the absolute fluorescence signals are sensitive to the variations in experimental conditions, there is a substantially limit in general applicability for generating consistent and stable readouts. Accordingly, the signal-to-noise ratio (SNR), defined as the ratio of ΔF (F – F0) between positive and negative reactions, was adopted as a robust metric to effectively normalize the background fluctuations (Lim et al., n.d.).

As the concentration of reaction probes plays a critical role in platform performance, it was prioritized for initial optimization. Systematic evaluation of the platform components revealed that 5 nM reaction probes (Fig. 2A) and 20 U T7 RNA polymerase (Fig. 2B) reached the optimal S/N ratio. The NTP dosage of 1 mM (Fig. 2C) and 20 nM RNP yielded the most robust signal response (Fig. 2D). In addition, the cascade probe concentration of 5 nM provided the maximum analytical performance (Fig. 2E). Additionally, we assessed the long-term storage stability of the cascade probes (Fig. S6). As depicted in Fig. S6, the engineered cascade probes demonstrated outstanding long-term stability and environmental resilience. Remarkably, the structural integrity and signal-transduction efficacy of the system were rigorously preserved even after prolonged storage and subjection to repeated freeze-thaw cycles. Finally, the buffer ratio of 0.5/0.5 and the reaction time of 30 min were selected as the optimal conditions (Fig. 2F). The detailed sequences were listed in Table S1, and all subsequent experiments were performed under these optimized conditions.

3.4. Analytical performance of the method

With this optimized workflow, we then evaluated assay performance under varied concentrations of target by end-point fluorescence and kinetic profiles. As shown in Fig. 3A and B, although it remained challenging to quantify the concentration of the target, the assay exhibited exceptional discriminatory capability between positive and negative groups. Notably, strong signals were observed even at low concentrations (e.g., 6×10^4 copies/μL), this phenomenon may attributable to the breathing dynamics of the cascade probe and stochastic collateral cleavage activity of Cas13a. Conversely, at moderate target concentrations (e.g., 6×10^6 copies/μL), competitive hybridization between the probe and the target strand may partially impair the efficiency of TWJ assembly, hence decreasing the concentration of the effective transcription template. The activated Cas13a can simultaneously cleave intermediate nucleic acid strands in the cascade reaction, disrupting cascading amplification and diminishing signal accumulation. Previous kinetic analyses have also suggested that reporter degradation and nonspecific cleavage could impose a fundamental limit on the sensitivity of CRISPR diagnostics, further contributing to nonlinear responses.

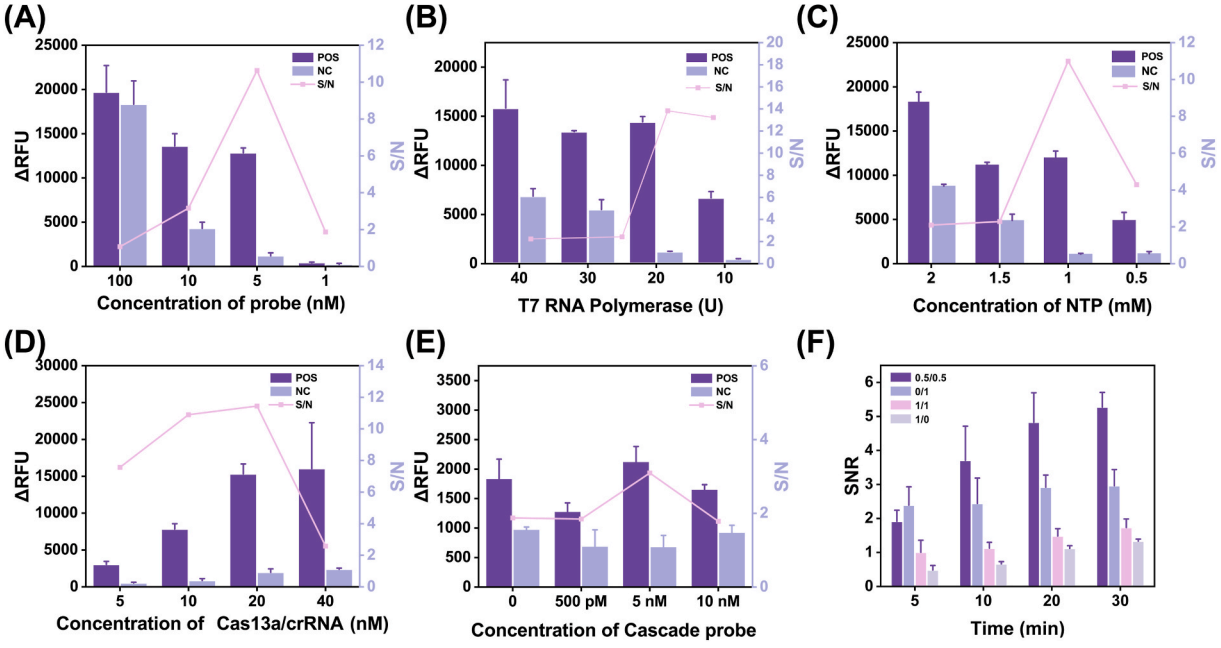


Fig. 2. Optimization of the reaction system. (A) Optimization of the concentration of the reaction probes (SP1/SP2/ST). (B) Optimization of the concentration of T7 RNA polymerase employed in the transcription. (C) Effect of NTP concentration with probe concentration fixed at 5 nM. (D) Optimization of RNP concentration under established conditions. (E) Concentration of cascade probe was tested under the optimized condition. (F) End-point fluorescence across four reaction buffers with 6×10^6 copies/μL HBB. The highest S/N was obtained at a buffer ratio of 0.5/0.5. Error bars: standard deviation (SD), n = 3.

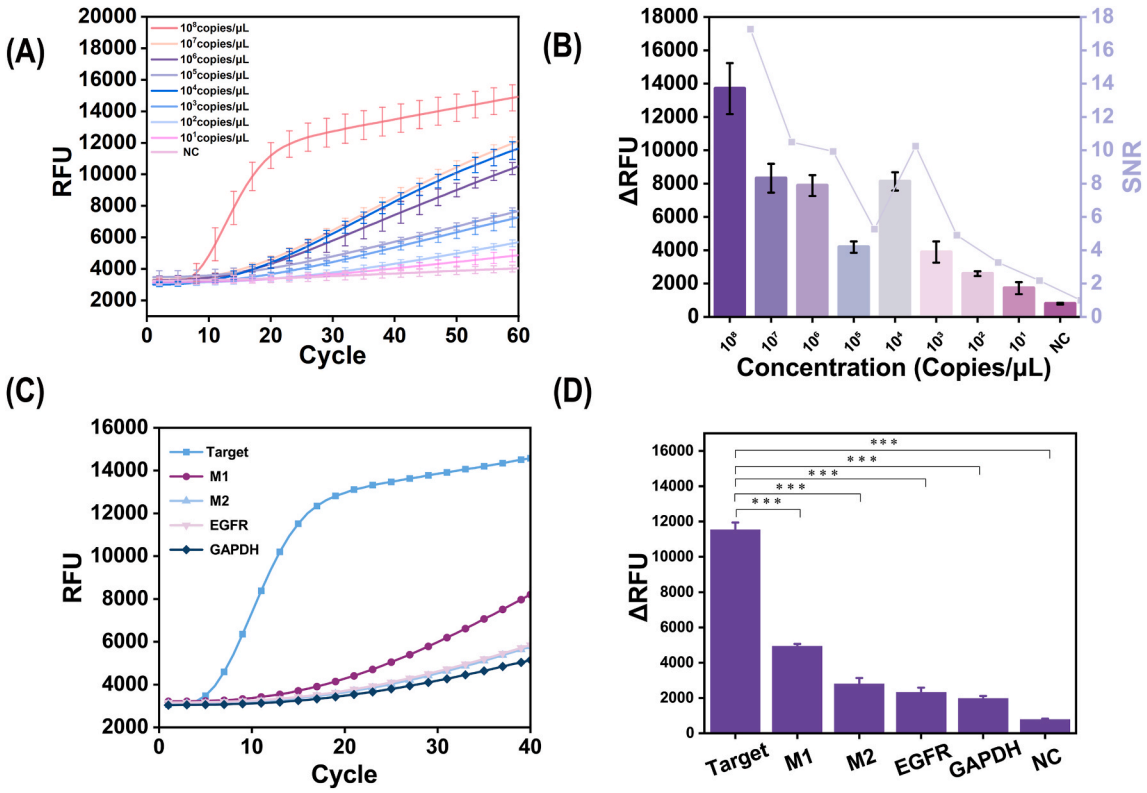


Fig. 3. Analytical performance of the method. (A–B) The cascade reaction achieved a detection limit of 10 copies/μL. (C–D) Selectivity evaluation of the method. The concentrations of single-base mutant HBB (M1), double-base mutant HBB (M2), EGFR, and GAPDH were each 6×10^{10} copies/μL, while HBB was set at 6×10^{9} copies/μL (*p < 0.05, **<0.01, ***p < 0.001). Error bars: standard deviation (SD), n = 3.

Owing to the enzyme turnover and trans-cleavage reactions, analogous nonlinear dynamic behavior has been extensively documented in CRISPR-based detection circuits (Lim, n.d.).

Since the sequence mutation in mRNA can compromise the specificity of detection platforms, we assessed the specificity of the method. A panel of control groups was employed, including single-base mutant HBB (M1), double-base mutant HBB (M2) and two mRNAs (EGFR and GAPDH) which were also highly expressed in invasive breast cancer cell lines (Detsika et al., 2025; Ponzetti et al., 2017; Shi et al., 2017). As depicted in Fig. 3C and 3D, the fluorescence signal of M1 decreased by more than 50% relative to HBB, whereas M2 showed no discernible difference from the blank control. In addition, the two high-level mRNA controls (EGFR and GAPDH) produced negligible signals. These results demonstrate high selectivity of the platform.

In addition, we compared the fluorescence signals of the Target and M1 groups relative to the NC group. As shown in Fig. S7, the fluorescence signal of the Target group was significantly higher than that of the NC group ($P < 0.001$), confirming the efficient activation of the proposed system by the perfectly matched target sequence. Notably, although the M1 group containing a single-base mismatch also exhibited a significantly higher fluorescence signal than the NC group ($P < 0.001$), the target concentration used in the M1 group was 10-fold higher than that in the perfectly matched Target group (6×10^{10} copies/μL vs. 6×10^{9} copies/μL). Despite this substantial concentration advantage, the fluorescence intensity of the M1 group remained significantly lower than that of the Target group ($P < 0.001$), suggesting that the signal generated by the mismatched sequence was mainly attributed to limited nonspecific activation rather than efficient target recognition. These results demonstrate that the proposed platform maintains high sequence discrimination capability, even under stringent mismatch conditions involving an excess amount of non-perfectly matched target sequences.

3.5. Cascade-based detection of HBB, CD55, and KRT17 with high sensitivity

To further demonstrate the applicability, we established cascade detection platforms for three breast cancer-associated mRNA targets (HBB, CD55, and KRT17). We identified the specific TWJ probe and cascade probe sequences for each target and developed corresponding assays. During assay development, detection of 0.6 copies/μL target demonstrated the high sensitivity of the CRISPR-Cascade system. Notably, across target concentrations from 0.6 to 6×10^{2} copies/μL, the SNR for each target consistently ranged from 1.6 to 3.5, exhibiting reliable target identification at low abundance (Fig. 4A–F). Compared with previous studies (e.g., Lim et al.), the proposed platform exhibited a greater signal-to-background separation within a 30 min reaction time, enabling more reliable discrimination between target and control samples.

3.6. Analysis of cell lines

As previously reported, HBB is highly expressed in invasive breast cancer cells (Ponzetti et al., 2017). To further evaluate the practical applicability of the proposed method, we profiled the relative mRNA expression levels of HBB, CD55, and KRT17 in non-invasive (MCF-7) and invasive (MDA-MB-231) breast cancer cell lines, using β-actin as an internal reference. The relative expression was defined as the ratio of target to reference fluorescence signals. As shown in Fig. 5B, the fluorescence signal observed in MDA-MB-231 cells was significantly higher than that in MCF-7 cells, indicating that the expression of these biomarkers was upregulated in invasive cells. Furthermore, the performance of the TCCA platform showed strong concordance with RT-qPCR results (Fig. 5A), supporting the reliability and potential for clinical application.

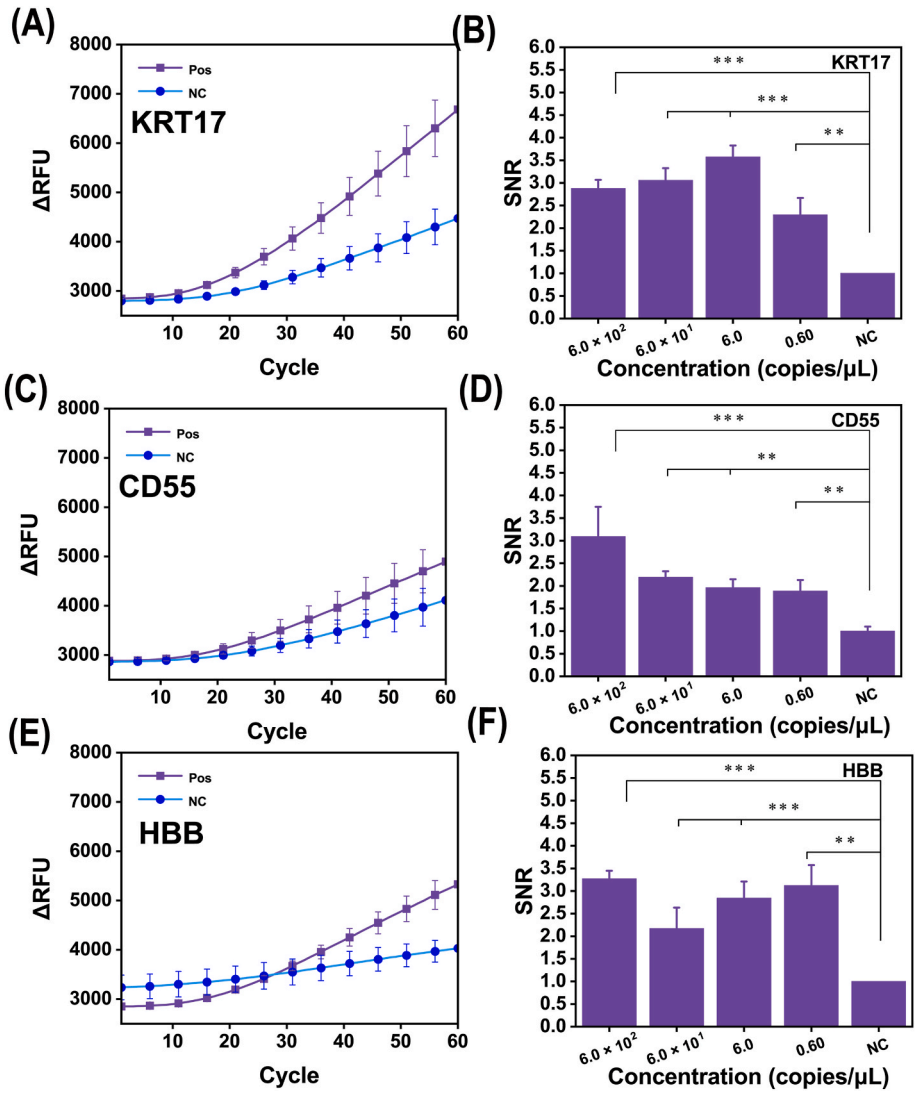


Fig. 4. Cascade assay for detecting different breast cancer biomarkers. (A, C, and E) Real-time fluorescence results at 0.6 copies/μL different target after 30 min, showing positive and negative responses for different targets: (A) KRT17, (C) CD55, and (E) HBB. (B, D, and F) Corresponding Signal-to-noise ratios at 30 min for target concentrations ranging from 0.6 to 6 × 10^3 copies/μL in water: (B) KRT17, (D) CD55, and (F) HBB. Error bars: standard deviation (SD), n = 3.

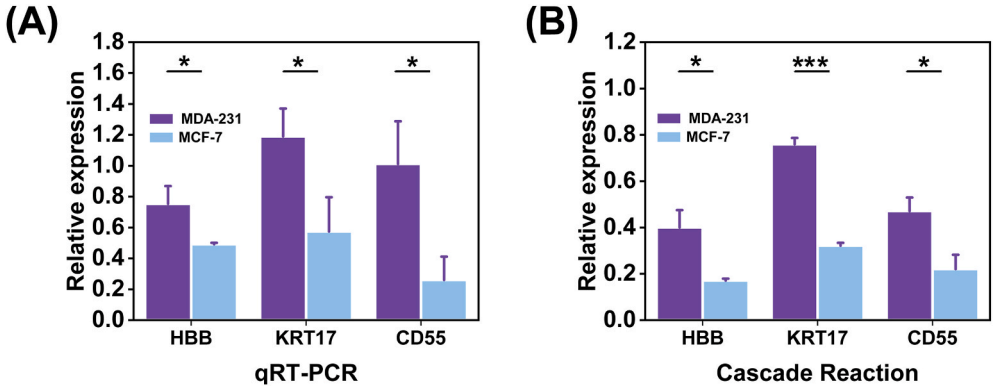


Fig. 5. Relative expression levels of HBB, CD55, and KRT17 in MCF-7 and MDA-MB-231 cell lines were measured by RT-qPCR and TCCA (*p < 0.05, ***p < 0.001). All data are presented as the mean ± SD from three independent experiments (n = 3).

3.7. OR-gate functionality

The TWJ architecture shows a very high sequence recognition specificity, which is essentially driven by the strict thermodynamic requirements of cooperative hybridization (Lee et al., 2020; Robinson et al., 2026; Yoon et al., 2022). Unlike traditional linear probes, the formation of stable TWJ requires precise complementary hybridization across multiple structural arms, which effectively inhibits non-specific

interactions and can accurately distinguish highly homogeneous sequences or single-base mismatches. Thus, the inherent branching and modular characteristics of the TWJ structural basis sequence provide a reliable platform for multiple detection. Importantly, the implementation of this TWJ-based multiple detection not only significantly improves the overall detection efficiency and analysis throughput, but also minimizes the detection cost and operational effort. Thus, such a platform enables to provide a more comprehensive and highly reliable diagnostic for complex biological samples.

In view of these characteristics, we developed a multiplex OR logic-gated system capable of generating a positive signal upon recognition of any target biomarker at low abundance within a pool (Fig. 6A). This capability enables simultaneous detection of multiple breast cancer biomarkers, thereby improving diagnostic efficiency while reducing cost and analysis time. Although tissue biopsy remains the clinical gold standard for morphological and molecular characterization, it is time-consuming and limited in detecting low-abundance targets (Ma et al., 2024; Zhou et al., 2022). Particularly in early-stage invasive breast cancer, circulating nucleic acid biomarkers are typically present at fM to aM levels, underscoring the need for rapid multiplex mRNA detection to enable timely diagnosis and better resolve tumor heterogeneity.

Besides, as the expression of individual biomarkers may vary across different breast cancer subtypes and patients, reliance on a single biomarker may lead to false-negative results. HBB, CD55, and KRT17 represent complementary biological features associated with oxidative stress adaptation, immune evasion, and aggressive tumor phenotypes, respectively. Therefore, their combined detection through the OR-gate strategy improves detection robustness by mitigating the impact of expression heterogeneity, thereby enhancing the biological relevance and potential clinical utility of the proposed platform.

Then we evaluated the capability for the simultaneous detection of singleplex, duplex, and triplex target combinations. Three mRNAs (HBB, CD55, and KRT17) and their corresponding reaction probes (5 nM) were respectively assessed in one pot to evaluate the performance of multiple detection in practical application. As shown in Fig. 6B, the SNR values were first evaluated for individual detection of the three targets (HBB, CD55, and KRT17) at both 0.6 copies/μL and 6 copies/μL input levels. Each target produced a measurable fluorescence response, indicating that the proposed system was capable of detecting extremely low-abundance nucleic acids for these three targets. As the multiple targets were simultaneously introduced into one reaction mixture, a significantly enhanced SNR was observed compared with the signals obtained from individual targets. Besides, the triplex detection group generated the highest fluorescence response, suggesting that the simultaneous detection of targets can substantially amplify the overall signal output of the sensing system. In addition, we further compared the analytical performance of the singleplex and multiplex detection systems for individual targets to evaluate whether multiplexing compromises the analytical performance of the detection platform. As shown in Fig. S8, the multiplex assay exhibited amplification kinetics comparable to those of the corresponding singleplex assays. Although slight variations in fluorescence signals were observed at attomolar target concentrations, these differences can be attributed to the stochastic activation behavior at extremely low target concentrations and did not affect the clear discrimination from the negative control. Furthermore, both the singleplex and multiplex assays achieved the same limit of detection (LOD)

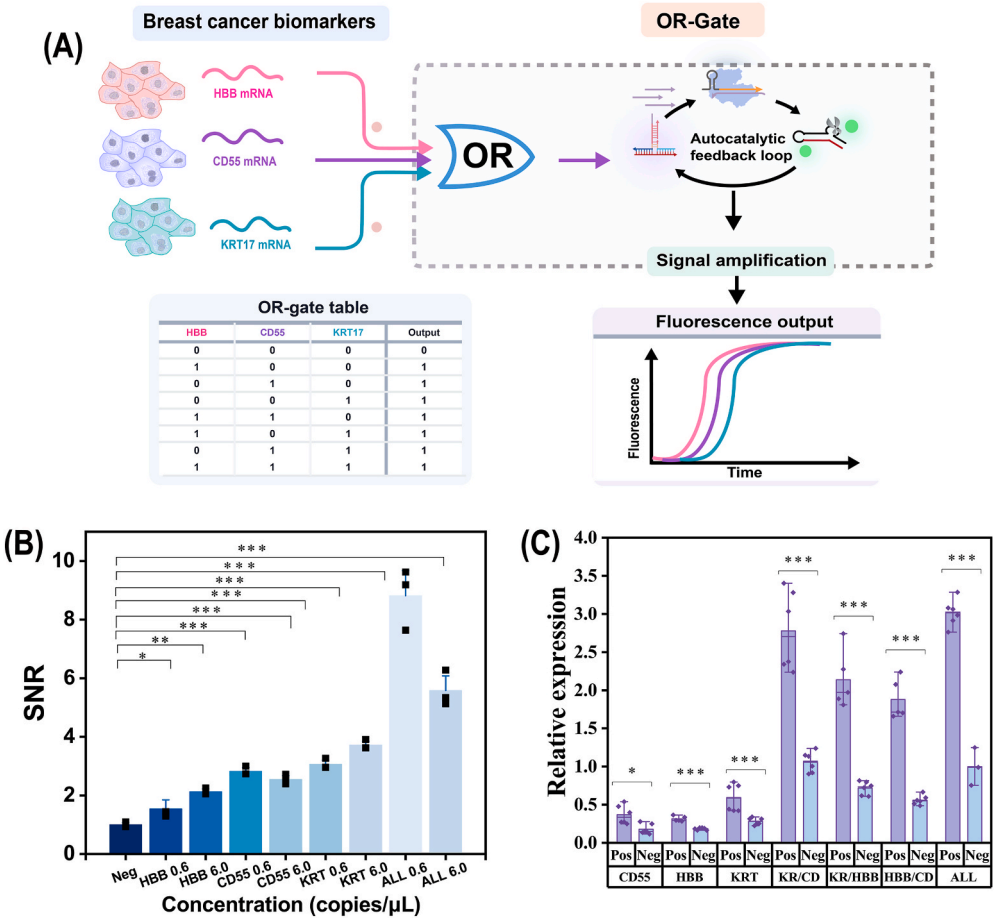


Fig. 6. Cascade amplification with OR-gated logic for breast cancer biomarker detection. (A) Schematic representation of an OR-function logic gate integrating three individual assays. (B) SNR results at 30 min for each target detection. (C) Multiplex detection of three targets in breast cancer cell lines (MDA-MB-231 and MCF-7). Error bars: standard deviation (SD), n = 3.

of 0.6 copies/μL. These results demonstrate that the OR-gate multiplex strategy maintains analytical performance comparable to that of singleplex detection while enabling simultaneous multi-target analysis. Besides, we further validated the multiplex detection performance of the platform in real biological samples. The low-expression cell line MCF-7 and the high-expression cell line MDA-MB-231 were used as negative and positive controls, respectively. Samples underwent extraction and purification using commercial kits, followed by analysis in a multiplex OR-gated CRISPR-Cascade assay. As shown in Fig. 6C, simultaneous detection of two or three targets in cell lines produced markedly higher signal intensities than single-target detection, indicating that parallel target recognition enhances detection reliability and analytical robustness. Above all, these results prove the proposed system suitable for multiplex biomarker detection in complex biological samples.

4. Discussion

Benefit from the programmability and predictability of Watson–-Crick base pairing together with the versatile molecular toolkit of enzymes, nucleic acids have evolved from simple hybridization probes into integrated platforms for biosensing, bioanalysis, and biomedical applications. Previous studies have demonstrated that conventional CRISPR/Cas13a systems are susceptible to nonspecific activation in complex environments and are limited by relatively low catalytic turnover rates. Despite this limitation, activated Cas13a can maintain prolonged collateral cleavage activity, thereby increasing the likelihood of unintended signal generation. In addition, current CRISPR cascade systems inherently constrained by the substrate specificity of Cas enzymes, which restricts their adaptability for broader applications.

Herein, we developed a platform based on target-induced proximity ligation assay coupled with split-T7 promoter-mediated transcription to regulate the reaction pathway. Unlike the strategy reported by Lim et al., in which target recognition directly initiates transcription through a preconfigured promoter architecture, our platform integrates target-induced proximity ligation with split-T7 promoter reconstitution, allowing transcription to occur only after successful junction assembly. This hierarchical reaction design introduces additional kinetic checkpoints, minimizes premature activation, and provides enhanced programmability for modular target recognition and signal regulation. According to kinetic gating, structural confinement of probes and integration of transcription-driven feedback modules, the controllability and signal fidelity of the platform are further improved. Compared with direct activation of Cas13a by target RNA, the TWJ-driven strategy introduces a target-guided junction structure that generates signal through transcription, leading to a stepwise activation mechanism. The transcription step serves as a thresholding mechanism, filtering transient or weak interactions and thereby reducing stochastic activation. In this framework, activation of Cas13a depends on the successful progression of these preceding steps, effectively introducing additional kinetic checkpoints. Due to the increased energetic barriers associated with conformational rearrangement, mismatched targets are less likely to proceed through this process, indicating that multi-step assembly processes enhance specificity by delaying enzyme activation and increasing reaction selectivity. Additionally, the introduction of a cascade probe to construct an autocatalytic feedback circuit dramatically increased the sensitivity, extending the limit from the 6×10^5 copies/μL to the 0.6 copies/μL range. Moreover, compared with most of the CRISPR-Dx methods, TCCA not only avoids extra target amplification step, but also decouples target recognition from signal transduction, enabling flexible reprogramming of the sensing module by alteration of the recognition sequence or incorporation of aptamer elements to accommodate diverse targets. Finally, the applicability of the platform was demonstrated through multiplex detection of breast cancer biomarkers.

Although the proposed platform enables highly sensitive detection, its current implementation is intended primarily for threshold-based sample classification rather than absolute quantification. The establishment of a fluorescence threshold using positive and negative controls allows reliable discrimination between positive and negative samples, which is adequate for identifying invasive and non-invasive breast cancer cell phenotypes in this study. The nonlinear signal amplification introduced by transcription and autocatalytic feedback may limit quantitative accuracy over a broad dynamic range. Therefore, future efforts will focus on optimizing reaction kinetics and incorporating quantitative calibration strategies to further enhance the quantitative performance of the platform.

As the analytical sensitivity reported in this study was determined using purified nucleic acid samples, future work will evaluate the performance of the platform in crude or minimally processed clinical validation samples to further assess its practical applicability.

Overall, the proposed CRISPR-cascade platform bypasses the inherent limitations of conventional Cas13a systems through an engineered internal positive feedback circuit for signal amplification. This design eliminates the need for conventional target nucleic acid amplification while enabling discrimination of single-nucleotide mismatches, with SNR >1.5 at a single target concentration of 0.6 copies/μL. The platform demonstrates broad applicability in detecting multiple breast cancer biomarkers (HBB, CD55, and KRT17) and incorporates an innovative multiplex OR-gated logic design to enable rapid and signal convergence for low-abundance targets. Overall, this study expands the methodological toolbox for CRISPR-Cas13a-based detection and provides a promising foundation for future molecular analysis applications.

CRediT authorship contribution statement

Yuqian Tan: Conceptualization, Data curation, Formal analysis, Investigation, Methodology, Validation, Writing – original draft, Writing – review & editing. **Xin He:** Data curation, Formal analysis, Investigation, Validation, Writing – original draft. **Erzhu Shao:** Conceptualization, Data curation. **Qiang Chen:** Formal analysis, Investigation. **Li Zhang:** Conceptualization, Funding acquisition, Methodology, Supervision, Writing – original draft, Writing – review & editing. **Shixiong Deng:** Funding acquisition, Supervision, Writing – review & editing.

Declaration of competing interest

The authors declare that they have no known competing financial interests or personal relationships that could have appeared to influence the work reported in this paper.

Acknowledgements

This research work was financially supported by the Natural Science Foundation of Chongqing Province (CSTB2025NSCQ-GPX1202).

Appendix A. Supplementary data

Supplementary data to this article can be found online at https://doi.org/10.1016/j.bios.2026.119049.

Data availability

Data will be made available on request.

References

Aslan, Y., Taşkın Korucu, Y., Day, B., Yılmaz, R., 2026. Development of a gold nanoparticle-based amplification-free nanobiosensor for rapid DNA detection supported by machine learning. Biosensors (Basel) 16, 128. https://doi.org/10.3390/bios16020128.

Detsika, M.G., Sakkou, M., Triantafyllidou, V., Konstantopoulos, D., Grigoriou, E., Psarra, K., Jahaj, E., Dimopoulou, I., Orfanos, S.E., Tsirogianni, A., Kollias, G., Kotanidou, A., 2025. CD55 upregulation in T cells of COVID-19 patients suppresses type-I interferon responses. Commun. Biol. 8, 690. https://doi.org/10.1038/s42003-025-08066-z.

Fakhr, Z.A., Xie, W., Zeng, S., Cai, S., 2026. Site accessibility-driven CRISPR/Cas13a activation for amplification-free RNA biosensing. Anal. Chim. Acta 1383, 344858. https://doi.org/10.1016/j.aca.2025.344858.

Gholamalipour, Y., Karunanayake Mudiyanselage, A., Martin, C.T., 2018. 3′ end additions by T7 RNA polymerase are RNA self-templated, distributive and diverse in character—RNA-Seq analyses. Nucleic Acids Res. 46, 9253–9263. https://doi.org/10.1093/nar/gky796.

He, D., Zhao, S., Wang, F., Wu, B., Wei, F., Zhao, Y., Wei, X., Ren, H., Zhang, M., Fan, Y., Zhang, J., Yu, S., Tang, Y., Diao, Y., 2025. H9N2 avian influenza virus diagnostics utilizing specific high-sensitivity enzymatic molecular system termed RPA-based CRISPR-Cas13a. Int. J. Biol. Macromol. 301, 140474. https://doi.org/10.1016/j.ijbiomac.2025.140474.

Hohmann, L., Nacer, D.F., Aine, M., Memari, Y., Black, D., Bowden, R., Davies, H.R., Borg, Å., Vallon-Christersson, J., Nik-Zainal, S., Staaf, J., 2025. Molecular profiling of the Basal-like intrinsic molecular subtype in primary ER-positive HER2-negative breast cancer. Genome Med. 17, 146. https://doi.org/10.1186/s13073-025-01576-9.

Huyke, D.A., Ramachandran, A., Bashkirov, V.I., Kotseroglou, E.K., Kotseroglou, T., Santiago, J.G., 2022. Enzyme kinetics and detector sensitivity determine limits of detection of amplification-free CRISPR-Cas12 and CRISPR-Cas13 diagnostics. Anal. Chem. 94, 9826–9834. https://doi.org/10.1021/acs.analchem.2c01670.

Kim, D., Kim, J., Han, J., Shin, J., Park, K.S., 2024. Split T7 switch-mediated cell-free protein synthesis system for detecting target nucleic acids. Biosens. Bioelectron. 261, 116517. https://doi.org/10.1016/j.bios.2024.116517.

Kreitmann, L., Miglietta, L., Xu, K., Malpartida-Cardenas, K., D'Souza, G., Kaforou, M., Brengel-Pesce, K., Drazek, L., Holmes, A., Rodriguez-Manzano, J., 2023. Next-generation molecular diagnostics: leveraging digital technologies to enhance multiplexing in real-time PCR. Trends Anal. Chem. 160, 116963. https://doi.org/10.1016/j.trac.2023.116963.

Lee, S., Jang, H., Kim, H.Y., Park, H.G., 2020. Three-way junction-induced isothermal amplification for nucleic acid detection. Biosens. Bioelectron. 147, 111762. https://doi.org/10.1016/j.bios.2019.111762.

Li, D., Cheng, W., Yin, F., Yao, Y., Wang, Z., Xiang, Y., 2025. A sensitive miRNA detection method based on a split-T7 switch modulating CRISPR/Cas12a system. Chem. Commun. 61, 4555–4558. https://doi.org/10.1039/D5CC00170F.

Lim, J., Van, A.B., Koprowski, K., Wester, M., Valera, E., Bashir, R., n.d. Amplification-free, OR-gated CRISPR-Cascade reaction for pathogen detection in blood samples. Proc. Natl. Acad. Sci. U. S. A. 122, e2420166122. https://doi.org/10.1073/pnas.2420166122.

Lim, J., n.d. Amplification-free dual-blocking autocatalytic CRISPR-Cascade for atto-molar DNA detection with low nonspecific Signal. https://doi.org/10.64898/2025.12.03.692097.

Ma, L., Guo, H., Zhao, Y., Liu, Z., Wang, C., Bu, J., Sun, T., Wei, J., 2024. Liquid biopsy in cancer: current status, challenges and future prospects. Signal Transduct. Targeted Ther. 9, 336. https://doi.org/10.1038/s41392-024-02021-w.

Ponzetti, M., Capulli, M., Angelucci, A., Ventura, L., Monache, S.D., Mercurio, C., Calgani, A., Sanità, P., Teti, A., Rucci, N., 2017. Non-conventional role of haemoglobin beta in breast malignancy. Br. J. Cancer 117, 994–1006. https://doi.org/10.1038/bjc.2017.247.

Robinson, N.E., Zhang, W., Ghosh, R., Gerber, B., Zhang, H., Sanfiorenzo, C., Wang, S., Di Carlo, D., Wang, K., 2026. Construction of complex and diverse DNA sequences using DNA three-way junctions. Nature 1–10. https://doi.org/10.1038/s41586-025-10006-0.

Schaffter, S.W., Green, L.N., Schneider, J., Subramanian, H.K.K., Schulman, R., Franco, E., 2018. T7 RNA polymerase non-specifically transcribes and induces disassembly of DNA nanostructures. Nucleic Acids Res. 46, 5332–5343. https://doi.org/10.1093/nar/gky283.

Shi, K., Xie, S., Tian, R., Wang, S., Lu, Q., Gao, D., Lei, C., Zhu, H., Nie, Z., 2021. A CRISPR-Cas autocatalysis-driven feedback amplification network for supersensitive DNA diagnostics. Sci. Adv. 7. https://doi.org/10.1126/sciadv.abc7802.

Shi, Y., Ye, P., Long, X., 2017. Differential expression profiles of the transcriptome in breast cancer cell lines revealed by next generation sequencing. Cell. Physiol. Biochem. 44, 804–816. https://doi.org/10.1159/000485344.

Son, S., Lyden, A., Ng, C.F., Dextre, A., Shu, J., Stephens, S.I., Fozouni, P., Knott, G.J., Smock, D.C.J., Liu, T.Y., Boehm, D., Simoneau, C., Kumar, G.R., Doudna, J.A., Ott, M., Fletcher, D.A., 2026. Programmable kinetic barcoding for multiplexed RNA detection with Cas13a. Nat. Biomed. Eng. 1–12. https://doi.org/10.1038/s41551-026-01642-6.

Tong, X., Zhang, K., Han, Y., Li, T., Duan, M., Ji, R., Wang, X., Zhou, X., Zhang, Y., Yin, H., 2024. Fast and sensitive CRISPR detection by minimized interference of target amplification. Nat. Chem. Biol. 20, 885–893. https://doi.org/10.1038/s41589-023-01534-9.

Wang, X., Zhong, L., Zhang, W., Wu, P., Wang, M., Li, D., Dong, L., Wang, G., 2025. CRISPR digital sensing: from micronano-collaborative chip to biomolecular detection. ACS Nano 19 (22), 20427–20451. https://doi.org/10.1021/acsnano.5c03474.

Yoon, T., Shin, J., Choi, H.-J., Park, K.S., 2022. Split T7 promoter-based isothermal transcription amplification for one-step fluorescence detection of SARS-CoV-2 and emerging variants. Biosens. Bioelectron. 208, 114221. https://doi.org/10.1016/j.bios.2022.114221.

Zadeh, J.N., Steenberg, C.D., Bois, J.S., Wolfe, B.R., Pierce, M.B., Khan, A.R., Dirks, R.M., Pierce, N.A., 2011. NUPACK: analysis and design of nucleic acid systems. J. Comput. Chem. 32, 170–173. https://doi.org/10.1002/jcc.21596.

Zhang, J., Li, L., Zhu, Y., Qian, K., Xu, Q., Qin, Y., Wu, L., 2025. Amplification-free CRISPR-Cas system integrated centrifugal digital microfluidic platform developed for multiplexed respiratory pathogen nucleic acid analysis. Anal. Chem. 97, 25583–25591. https://doi.org/10.1021/acs.analchem.5c04524.

Zhang, Y., Chen, Y., Zhang, Q., Liu, Y., Zhang, X., 2023. An aM-level sensitive cascade CRISPR-Dx system (ASCas) for rapid detection of RNA without pre-amplification. Biosens. Bioelectron. 230, 115248. https://doi.org/10.1016/j.bios.2023.115248.

Zhao, S., Zhang, J., Yu, S., He, D., Li, B., Fan, Y., Liu, G., Tang, Y., Diao, Y., 2025. Integration of RPA and CRISPR-Cas13a collateral activity for one-step detection of DHAV-3: a biological macromolecule-enabled diagnostic platform. Int. J. Biol. Macromol. 314, 144400. https://doi.org/10.1016/j.ijbiomac.2025.144400.

Zhou, H., Zhu, L., Song, J., Wang, G., Li, P., Li, W., Luo, P., Sun, X., Wu, J., Liu, Y., Zhu, S., Zhang, Y., 2022. Liquid biopsy at the frontier of detection, prognosis and progression monitoring in colorectal cancer. Mol. Cancer 21, 86. https://doi.org/10.1186/s12943-022-01556-2.

Zhou, J., Li, Z., Seun Olajide, J., Wang, G., 2024. CRISPR/Cas-based nucleic acid detection strategies: trends and challenges. Heliyon 10, e26179. https://doi.org/10.1016/j.heliyon.2024.e26179.

Zhou, J., Zhang, N., Ren, Y., Ren, X., Wang, X., Gou, X., Goto, A., Ueki, S., Gopinath, S.C. B., Chen, K., Li, Z., 2026. Challenges and strategies for CRISPR-Cas molecular diagnostics from mechanism to clinical translation. Sens. Acutators Rep. 11, 100437. https://doi.org/10.1016/j.snr.2026.100437.